Structure of the $^6Li \rightarrow p+(n\alpha)$ vertex: $^6Li(p,2p)n\alpha$ reaction

C. T. Christou,* D. R. Lehman, and W. C. Parke
Department of Physics, The George Washington University, Washington, D.C. 20052
(Received 31 August 1987)

Three-body models of the ^6Li nucleus are used to derive the coincidence cross sections for the reaction $^6Li(p,2p)n\alpha$. It is shown that in the plane-wave impulse approximation, the fourfold differential cross section factorizes in such a way that the $^6Li \rightarrow p+(n\alpha)$ joint momentum distribution may be extracted from experimental measurements. The calculated results are compared to data from various $^6Li(p,2p)n\alpha$ experiments with incident energies ranging from 100 to 460 MeV. Differences between predictions of various three-body models and of various representations of the underlying two-body interactions are examined. It is concluded that meaningful comparisons are possible only if the beam energy is high enough to ensure proton pole dominance and the detector energy resolution good enough to distinguish crucial spectral features.

I. INTRODUCTION

This paper is the second in a series of three dealing with the structure of the $^6Li \rightarrow p + (n\alpha)$ vertex, as predicted by a three-body model of the ^6Li nucleus. In Ref. 1, the three-body formalism of the $^6Li \rightarrow p + (n\alpha)$ overlap amplitude is developed and the $p + (n\alpha)$ joint momentum distribution derived as a function of q, the momentum of the proton (p) with respect to the center of mass of the neutron-alpha ($n\alpha$) pair, and E_κ, the relative energy of the $n\alpha$ pair. The joint momentum distribution enters into the cross section for the $^6Li(p,2p)n\alpha$ coincidence reaction, which forms the subject of the present paper. Finally, Ref. 2 focuses on the $^6Li(e,e'p)n\alpha$ reaction in which electrons, rather than protons, are used as projectiles.

The ^6Li nucleus has been the object of both experimental and theoretical activities in the past thirty years because it is one of the lightest nuclei exhibiting substructures. The usefulness of coincidence reactions as a means of investigating single-particle properties of bound protons was first recognized by Jacob and Maris.[3] In particular, emphasis was placed on the use of protons and electrons as probes of the structure of light nuclei, for which distortion effects are expected to be relatively small. Since then, several $^6Li(p,2p)n\alpha$ experiments have been conducted, with the goal of extracting the momentum distribution of the least bound proton.

In the $^6Li(p,2p)n\alpha$ reaction, the incident particle scatters off a ^6Li nucleus, which then breaks up into an essentially freely moving proton and an interacting $n\alpha$ pair. The two outgoing protons are detected in coincidence for a series of scattering angles, θ. The fourfold cross section, $d^4\sigma/d\Omega_1 d\Omega_2 dE_1 dE_2$, is measured as a function of proton separation energy or, equivalently, E_κ, the excitation energy of the recoiling $n\alpha$ pair. This "binding energy spectrum" exhibits peaks corresponding to the resonant states of the pair. Integration of $d^4\sigma$ over a particular peak yields the threefold cross section, $d^3\sigma/d\Omega_1 d\Omega_2 dE_1$, which is expressed either as a function of q (energy sharing spectrum) or θ (angular correlation spectrum). The $p + (n\alpha)$ momentum distribution may be extracted from the former under conditions of proton pole dominance.

There is a disadvantage to using protons (versus electrons) as projectiles in that they interact strongly with each other as well as with the target nucleus. This renders the extraction of useful information from (p,2p) type reactions difficult, as the data are obscured by initial-state and final-state interactions that involve the projectile. There are two ways to minimize distortion effects in these experiments. One is by setting up a coplanar symmetric angle geometry (Fig. 1) in which the two detectors are placed at equal and opposite angles relative to the incident beam direction. Since lower energy protons are more strongly affected by distortion, it is expected that the use of such a geometry, with equal proton energies, will minimize distortion effects. In this case, $\mathbf{q}$ is parallel to $\mathbf{p}_0$ [Fig. 1(a)]. Figure 1(b) shows the case where $E_1 \neq E_2$, and $\mathbf{q}$ forms an angle $\psi \neq 0$ with $\mathbf{p}_0$. More importantly, however, distortion effects may be limited by increasing the beam energy to guarantee relatively high kinetic energies for both incoming and outgoing protons. The higher their kinetic energy, the faster the protons leave the region where the strong interaction is effective.

In all the experiments conducted to date, the data are characterized by the following consistent features:

(a) Two peaks in the binding energy spectrum, a sharp one at $E_\kappa \sim 0.7$ MeV corresponding to the $P_{3/2}$ $n\alpha$ resonance and a broader one at $E_\kappa \sim 16$ MeV arising from the $^6Li \rightarrow p + (d^3H)$ breakup channel;

(b) The absence of a minimum of zero at $q=0$ in the energy sharing spectrum and, as a result, in the $p + (n\alpha)$ momentum distribution.

The phenomenon described in (b) above contradicts the predictions of a pure p-shell model for the valence nucleons of the ^6Li nucleus, according to which the momentum distribution shows two symmetric peaks located around a minimum of zero. This has been inter-

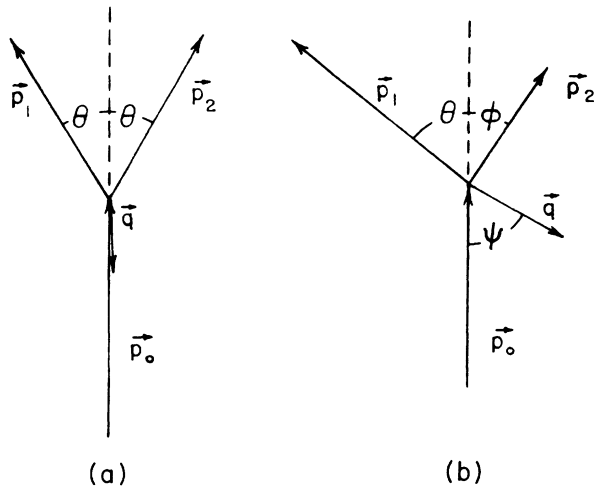

FIG. 1. Geometry of the ^{6}Li(p,2p)nα reaction.

preted, on the basis of the work of Saito *et al.*,[4] as arising from the presence of the $S_{1/2}$ nα interaction in the ground state of ^{6}Li, as well as the final rescattering nα state.

Unfortunately, the bulk of (p,2p) data suffers from distortion effects which complicate their meaningful interpretation. Therefore, comparisons with theoretical calculations which assume proton pole dominance serve only to confirm qualitative features, such as the shape of the momentum distribution, but not quantitative ones, such as the absolute magnitudes of cross sections.

Experiments which fall into this category are those of Garron *et al.*,[5] Tibell *et al.*,[6] Roynette *et al.*,[7] and MacKenzie *et al.*,[8] with incident energies all below 200 MeV and energy resolutions between 3.5 and 8.0 MeV. An exception is provided by the early work of Tyren *et al.*,[9] who conducted one of the first ^{6}Li(p,2p)nα experiments at a beam energy, E_0, of 460 MeV. In view of the relatively higher value of E_0, one would favor this set of data for purposes of comparison with theoretical results. Unfortunately, however, the information given by the authors is sparse. For instance, a knowledge of the energy resolution of the detectors is critical, since this must be folded into the theoretical cross section in order to compare with experiment. Tyren and coworkers do not report an energy resolution in their paper, although Roynette mentions a value of 3 MeV, which may have been obtained through a private communication. Uncertainty as to the energy resolution, however, makes any comparison tentative at best.

In addition, there are other omissions, such as the range of integration over E_κ used in the derivation of $d^3\sigma$. These shortcomings, in any case, do not detract from the overall quality of this work, and the good judgement of the experimentalists in using a relatively high beam energy.

The most recent ^{6}Li(p,2p)nα experiment was conducted by Bhowmik *et al.*[10] at the University of Maryland in 1974. A bombarding energy of 100 MeV was used and the two outgoing protons detected in coincidence for 17 angle pairs. Only for one such angle pair, in this case 42.8°, is the region around $q=0$ kinematically allowed. This value of θ is referred to as the quasifree scattering angle. As in previous experiments, the expected deep central minimum in the corresponding energy spectrum was mostly filled. This may be partially attributed to distortion, but the authors believe it is those wave function components originating from the underlying $S_{1/2}$ nα interaction that are mainly responsible. Again, it becomes obvious that the notion of a model in which the valence nucleons reside only in the 1p shell must be abandoned.

The data from the Maryland experiment are also plagued by distortion and rescattering effects, due to the low incident energy. However, the energy resolution is good (1 MeV) and the published spectra extensive. Comparison with theoretical results would serve as an indication of the importance of rescattering effects at 100 MeV. Also, qualitative features, such as the shapes of distributions as predicted by the pole-dominance assumption, may be verified. Unfortunately, there are no (p,2p) experiments to date with an incident energy high enough (>500 MeV) to ensure truly minimal distortion effects and an energy resolution good enough to distinguish crucial spectral features.

The most complete theoretical treatment of the ^{6}Li(p,2p)nα reaction to date is that of Saito, Hiura, and Tanaka.[4] Their study was based on an α-*d* cluster model and not a full treatment of the ^{6}Li nucleus as a three-body system. It has been shown, however, by Lehman and Rajan,[11] that the α-*d* component comprises only ~60% of the ground state of ^{6}Li, while the remaining 40% comes from the α + (np) configuration, which can only be analyzed on the basis of a three-body model. In spite of this limitation, however, the Saito treatment correctly regards the recoiling nα pair as an unbound system and includes the $S_{1/2}$ nα interaction in both the initial and final nuclear states. The relative α-*d* wave function used corresponds to a 2*s* state as required by the Pauli exclusion principle.

The p + (nα) momentum distribution was derived by Saito on the basis of the plane-wave impulse approximation (PWIA) for a final state in which the proton moves freely with respect to the rescattering nα pair. From this, angular distributions and summed energy spectra were computed and compared with the data of Roynette *et al.*[7] The theoretical calculations predicted consistently higher values (as much as 100%) than the experimental ones, which is not surprising since the beam energy was only 155 MeV and, therefore, distortion effects were non-negligible. The model did, however, correctly predict certain properties of the α-*d* configuration such as the small compressibility of the α-particle cluster, the weak binding of the two clusters, and the large root mean-square radius of ^{6}Li.

The partial minimum which appeared in the calculated p + (nα) momentum distribution was explained by Saito as originating from $S_{1/2}$ partial-wave components in the alpha-nucleon interaction. The effect of the plane-wave component, which represents the case where the two particles move freely, was included but not analyzed separately. Misled by "Watson's model",[12]

perhaps, theorists ignored the possibility that this component contribution may be significant, at least in certain regions of q. Failure to understand the importance of the plane-wave component turns out to be, as we shall see, critical. Aside from this, the significance of Saito's work lies in the fact that he moved away from the naive shell model toward a more realistic picture of the ^{6}Li nucleus as a few-body system.

Calculations based on the Saito model were also performed by Chang and coworkers[13] in order to estimate the contribution of S-wave knockout in the ^{6}Li(p,2p)nα and ^{6}Li(p,pn)pα reactions. Results were compared to the data extracted from the Bhowmik experiment, which has already been discussed. Their PWIA calculations overestimated the cross sections by as much as 50%, which again may be attributed to the value of the incident energy, 100 MeV, being too low to preclude rescattering effects. Like Saito, Chang concludes that the observed partial minimum in the p + (nα) momentum distribution arises from the $S_{1/2}$ nα partial-wave interaction in the ^{6}Li nucleus. The analysis is careful, but the approach does not go beyond that of Saito.

A theoretical derivation of the ^{6}Li(p,2p)nα cross section in the PWIA was also carried out at about the same time by Prats.[14] He compiled data from various (p,2p) experiments,[5–9] with incident energies ranging from 100 to 460 MeV and compared them to his calculation of the p + (nα) momentum distribution. Prats' motivation was to show that distortion effects do not play an important role in the ^{6}Li(p,2p)nα reaction, even at energies as low as 100 MeV. The comparison, however, must be considered inconclusive for two main reasons:

(a) Prats' treatment was based on phenomenological forms for the breakup vertex functions, with parameters fit to experimental data,

(b) Only the dominant $S_{1/2}$, $P_{3/2}$, $P_{1/2}$, and $D_{3/2}$ final state interactions were considered, ignoring the plane-wave component on the assumption that it contributes negligibly in the neighborhood of a resonance.

Prats' main statement is that the $S_{1/2}$ interaction is important in the nα system, while he recognizes that a complete three-body model approach is necessary to give a better understanding of the dynamics of the ^{6}Li nucleus.

The motivation behind our work was to go beyond existing theoretical treatments of the ^{6}Li$\rightarrow$p + (nα) breakup vertex by visualizing the ^{6}Li nucleus as a three-body system. This paper describes this work as applied to the ^{6}Li(p,2p)nα reaction and also compares our results to the available experimental data. The effectiveness of (p,2p) experiments is examined, and the conditions under which useful information can be extracted from them are explored. Such information would include the relative contributions of the various underlying two-body interactions to the shape and magnitude of the p + (nα) momentum distribution, as well as a determination of the most appropriate representations of these interactions. The ^{6}Li(p,2p)nα cross sections are derived in Sec. II, Sec. III presents the results of the comparisons, as well as a pertinent discussion, and Sec. IV includes a brief summary of the work and the main conclusions drawn from it.

II. ^{6}Li(p,2p)nα CROSS SECTIONS

A. Derivation

In the plane-wave impulse approximation (PWIA) to breakup reactions, the incoming particle is assumed to have interacted with only one nucleon, that which is detected. Kinetic energies must be high enough so that the motion of the incident particle, as well as both detected particles, may be described by plane waves. In the (p,2p) reaction, the incident proton strikes a nuclear proton and ejects it, immediately scattering away with no further interaction. This is equivalent to the assumption of proton pole dominance, a necessary condition, as we shall see, to the extraction of the p + (nα) momentum distribution from the experimental cross section.

The Feynman pole graph for the ^{6}Li(p,2p)nα reaction is shown in Fig. 2. Variables in parentheses refer to the energies and momenta of the respective particles. For the nα pair, q, the center-of-mass (c.m.) momentum, is equal to $\mathbf{k}_\alpha+\mathbf{k}_n$, while the relative momentum $\boldsymbol{\kappa}$ equals $\mathbf{k}_\alpha/5-4\mathbf{k}_n/5$ and the relative energy, E_κ, is $5\kappa^2/8M$, where M represents the nucleon mass. The ^{6}Li nucleus is stationary in the laboratory frame.

According to the guidelines of Feynman[15] and Shapiro,[16] the cross section may be set up as follows:

$$\sigma=\tfrac{1}{6}\int\left[\frac{1}{v_{\rm rel}}\sum_{\substack{m_0,m_1\\ m_2,m_n\\ m_6}}|\mathcal{M}(m_0,m_1,m_2,m_n,m_6)|^2\,\delta(E_0-B_6-E_1-E_2-E_n-E_\alpha)\right.$$
$$\left.\times(2\pi)^4\delta(\mathbf{p}_0-\mathbf{p}_1-\mathbf{p}_2-\mathbf{q})\frac{1}{(2\pi)^{12}}d^3p_1d^3p_2d^3p_nd^3p_\alpha\right], \qquad (1)$$

where the square of the amplitude of the reaction, $|\mathcal{M}(m_0,m_1,m_2,m_n,m_6)|^2$, is averaged over initial and summed over final spin states for unpolarized beams and targets. The spin quantum numbers are represented by m_0,m_1,m_2 for the incoming and outgoing protons, m_n for the neutron, and m_6 for ^{6}Li. The relative velocity of

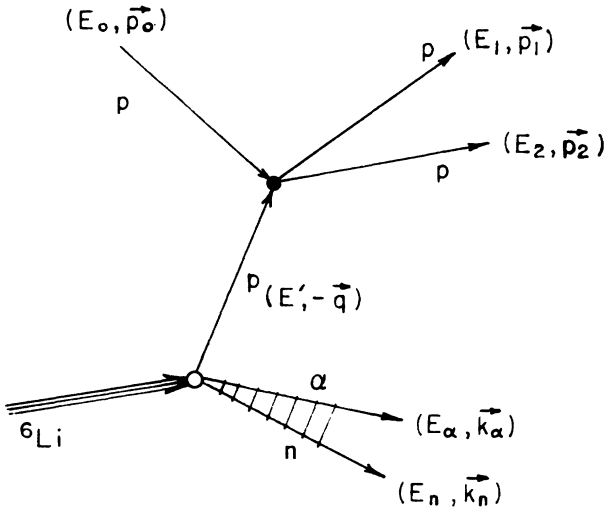

FIG. 2. The ^{6}Li(p,2p)nα reaction in pole dominance.

the incident proton and the target nucleus is p_0/E_0 in the laboratory frame.

We first reexpress the phase space elements in terms of $\mathbf{q}$ and κ,

$$d^3p_n d^3p_\alpha = d^3q\, d^3\kappa \ , \tag{2a}$$

and the energy δ function in terms of the magnitude of κ,

$$E_\kappa = \frac{5}{8}\frac{\kappa^2}{M} \ , \tag{2b}$$

$$\delta(E_\kappa - \cdots) = \frac{\delta(\kappa - \cdots)}{(\frac{5}{4})M\kappa} \ . \tag{2c}$$

The fourfold cross section is then obtained by integration over d^3q and $d\kappa$,

$$\frac{d^4\sigma}{d\Omega_1 d\Omega_2 dE_1 dE_2} = \frac{1}{6(2\pi)^8}\int \frac{E_0}{p_0}\sum_{\substack{m_0,m_1\\ m_2,m_n\\ m_6}} |\mathcal{M}|^2 \tfrac{4}{5} M\kappa E_1 p_1 E_2 p_2 d\Omega_{\hat{\kappa}} \ , \tag{3}$$

where $\Omega_{\hat{\kappa}}$ represents the angle of the unit vector $\hat{\kappa}$ in a frame where $\mathbf{q}$ lies in the z direction. To obtain the three-fold cross section, we rewrite the energy δ function in terms of the momentum p_2, then integrate over dp_2 and d^3q:

$$\delta(E_2 - \cdots) = \frac{\delta(p_2 - \cdots)}{\left|\dfrac{p_2}{E_2} - \dfrac{\hat{\mathbf{p}}_2\cdot(\mathbf{p}_0 - \mathbf{p}_1 - \mathbf{p}_2)}{E_q}\right|} \ , \tag{4a}$$

$$\frac{d^3\sigma}{d\Omega_1 d\Omega_2 dE_1} = \tfrac{1}{6}\int \frac{E_0}{p_0}\sum_{\substack{m_0,m_1\\ m_2,m_n\\ m_6}} \frac{|\mathcal{M}|^2 p_2^2 E_2 E_q E_1 p_1 d^3\kappa}{|E_q p_2 + p_2 E_2 - E_2\hat{\mathbf{p}}_2\cdot(\mathbf{p}_0 - \mathbf{p}_2)|} \ , \tag{4b}$$

since

$$p_1^2 dp_1 = E_1 p_1 dE_1 \ . \tag{4c}$$

The pp kinematics were treated relativistically to allow for high incident energies, while the ^{6}Li vertex kinematics were treated nonrelativistically because of the heavier recoiling nuclear mass and the low values of q and E_κ.

The amplitude $\mathcal{M}(m_0,m_1,m_2,m_n,m_6)$ may be written in terms of the pp and ^{6}Li breakup vertex amplitudes, M_{pp} and M:

$$\mathcal{M}(m_0,m_1,m_2,m_n,m_6) = \sum_{m_{p'}} \frac{M_{pp}(m_0,m_{p'},m_1,m_2)M(m_6,m_n,m_{p'})}{(E' + i\epsilon - q^2/2M)} \tag{5}$$

where the denominator is the proton propagator and the summation runs over the spin quantum numbers of the exchanged proton ($m_{p'}$).

Applying momentum and energy conservation to both vertices, we get for vertex 1:

$$-\mathbf{q} + \mathbf{p}_0 = \mathbf{p}_1 + \mathbf{p}_2 \ , \tag{6a}$$

$$E' + E_0 = E_1 + E_2 \ , \tag{6b}$$

and for vertex 2:

$$\mathbf{p}' + \mathbf{q} = -\mathbf{q} + \mathbf{q} \ , \tag{6c}$$

$$-B_6 = E' + \frac{q^2}{10M} + \frac{\kappa^2}{2\mu_{n\alpha}} \ , \tag{6d}$$

where $\mu_{n\alpha}$ is the nα reduced mass and B_6 the binding energy of the ^{6}Li nucleus, experimentally determined to be 3.7 MeV. The ^{6}Li→p + (nα) vertex amplitude is the matrix element, between initial and final states, of $V_{p\alpha} + V_{pn}$, the interaction term between the proton and the five nucleons (the term which is excluded in the final state):[1]

$$M(m_6,m_n,m_{p'}) = \langle -\mathbf{q}, m_{p'}, m_n, \varphi_\kappa^{(-)}(\mathbf{k}_{23}) | V_{p\alpha} + V_{pn} | \Psi_{m_6}^{[1]} \rangle \ . \tag{7}$$

In the above equation, $\varphi_\kappa^{(-)}(\mathbf{k}_{23})$ represents the nα scattering state wave function and $\Psi_{m_6}^{[1]}$ the ground state wave function of ^{6}Li. The Hamiltonian of the six nucleons can be written as a sum of the nα subchannel Hamiltonian plus H_0, the kinetic energy term of the p + (nα) relative motion, and $V_{p\alpha} + V_{pn}$. We therefore have

$$\langle -\mathbf{q}, m_{p'}, m_n, \varphi_\kappa^{(-)}(\mathbf{k}_{23}) \mid V_{p\alpha} + V_{pn} \mid \Psi_{m_6}^{[1]} \rangle$$
$$= -\left[B_6 + \frac{q^2}{2\mu_{p,n\alpha}} + \frac{\kappa^2}{2\mu_{n\alpha}} \right] \times \langle -\mathbf{q}, m_{p'}, m_n, \varphi_\kappa^{(-)}(\mathbf{k}_{23}) \mid \Psi_{m_6}^{[1]} \rangle , \quad (8)$$

where the reduced proton-(nα) mass, $\mu_{p,n\alpha}$, is $5M/6$.

Now, from Eq. (6d) we see that

$$\frac{q^2}{2M} - E' = B_6 + \frac{\kappa^2}{2\mu_{n\alpha}} + \frac{6}{10}\frac{q^2}{M} , \quad (9)$$

so that the propagator in Eq. (5) is canceled by the expression in parentheses in Eq. (8), a purely negative quantity. The expression for $\mathcal{M}(m_0, m_1, m_2, m_n, m_6)$ thus becomes

$$\mathcal{M}(m_0, m_1, m_2, m_n, m_6) = \sum_{m_{p'}} M_{pp}(m_0, m_{p'}, m_1, m_2) A(m_{p'}, m_n, m_6) , \quad (10)$$

where we have made the substitution

$$A(m_{p'}, m_n, m_6) = \langle -\mathbf{q}, m_{p'}, m_n, \varphi_\kappa^{(-)}(\mathbf{k}_{23}) \mid \Psi_{m_6}^{[1]} \rangle . \quad (11)$$

The left-hand side of Eq. (11) is the overlap of the ^{6}Li ground state wave function with the final state wave function.

By holding $\mathbf{q}$ along the z axis, it is straightforward to show that

$$\int d\Omega_{\hat{\kappa}} \tfrac{1}{3} \sum_{m_n, m_6} A^\dagger(\mathbf{q}, \kappa; m_p, m_n, m_6) A(\mathbf{q}, \kappa; m_{p'}, m_n, m_6) = \frac{\delta_{m_p, m_{p'}}}{2} V(\kappa, q) , \quad (12)$$

where $V(\kappa, q)$ is the joint momentum distribution [see Eqs. (20) and (21) of Ref. 1]. As a result, the absolute magnitude squared of the overall amplitude factorizes as follows:

$$\int \sum_{\substack{m_0, m_1 \\ m_2, m_n \\ m_6}} \left[\left| \sum_{m_p} M_{pp}(m_0, m_p, m_1, m_2) A(m_p, m_n, m_6) \right|^2 \right] d\Omega_{\hat{\kappa}} = \tfrac{1}{2} \sum_{\substack{m_0, m_1 \\ m_p, m_2}} |M_{pp}(m_p)|^2 \int \sum_{\substack{m_p, m_n \\ m_6}} |A(m_p, m_n, m_6)|^2 d\Omega_{\hat{\kappa}} . \quad (13)$$

In order to express $|M_{pp}|^2$ in terms of the elastic scattering cross section of two protons in their c.m. frame, $[d\sigma/d\tilde{\Omega}]_{pp}$, we consider the reaction $p_0 + p \rightarrow p_1 + p_2$ at vertex 1 (Fig. 2) and apply Shapiro's rules again to obtain:

$$\sigma = \tfrac{1}{4} \sum_{\substack{m_0, m_{p'} \\ m_1, m_2}} \int \frac{1}{v_{rel}} |M_{pp}(m_0, m_{p'}, m_1, m_2)|^2 \times \delta(\mathbf{p}_0 - \mathbf{q} - \mathbf{p}_1 - \mathbf{p}_2)(2\pi)^4 \times \delta(E_0 + E' - E_1 - E_2) \frac{d^3p_1}{(2\pi)^3} \frac{d^3p_2}{(2\pi)^3} . \quad (14)$$

In this notation, a tilde ($\sim$) over a quantity means that the quantity is calculated in the c.m. system.

Rewriting the energy δ function in Eq. (14) in terms of p_1, we have

$$\delta(E_1 - \cdots) = \frac{\delta(p_1 \cdots)}{\left| \frac{\mathbf{p}_1}{E_1} - \frac{\hat{\mathbf{p}}_1 \cdot (\mathbf{p}_0 - \mathbf{q} - \mathbf{p}_1)}{E_2} \right|} \quad \text{(lab frame)} , \quad (15a)$$

$$\delta(E_1 - \cdots) = \frac{\delta(p_1 \ldots)\tilde{E}_1\tilde{E}_2}{\tilde{p}_1(\tilde{E}_1 + \tilde{E}_2)} \quad \text{(pp c.m. frame)} . \quad (15b)$$

Integration over d^3p_2 and d^3p_1, gives

$$\frac{d\sigma}{d\tilde{\Omega}} = \frac{1}{(2\pi)^2} \tfrac{1}{4} \sum_{\substack{m_0, m_{p'} \\ m_1, m_2}} \frac{|M_{pp}(m_0, m_{p'}, m_1, m_2)|^2}{\tilde{p}_0\tilde{p}_1(\tilde{E}_0 + \tilde{E}')^2} \times \tilde{E}_1\tilde{E}_2\tilde{E}_0\tilde{E}'\tilde{p}_1^2 , \quad (16)$$

and

$$\tfrac{1}{4} \sum_{\substack{m_0, m_{p'} \\ m_1, m_2}} |M_{pp}(m_0, m_{p'}, m_1, m_2)|^2 = \frac{d\sigma}{d\tilde{\Omega}} \frac{(2\pi)^2\tilde{p}_0(\tilde{E}_0 + \tilde{E}')^2}{\tilde{p}_1\tilde{E}_1\tilde{E}_2\tilde{E}_0\tilde{E}'} . \quad (17)$$

Taking into account the relativistic invariance of

$$|M_{pp}|^2\tilde{E}_1\tilde{E}_2\tilde{E}_0\tilde{E}' ,$$

we finally obtain for the binding energy spectrum

$$\frac{d^4\sigma}{d\Omega_1 d\Omega_2 dE_1 dE_2}=\frac{1}{(2\pi)^6}\frac{1}{3}\int\left[\frac{\tilde{p}_0 p_1 p_2(\tilde{E}_0+\tilde{E}\,')^2 4M\kappa}{5}\right]\left[\frac{d\sigma}{d\tilde{\Omega}}\right]_{pp}\sum_{\substack{m_n,m_{p'}\\ m_6}}|A|^2 d\Omega_{\hat{\kappa}}\,, \tag{18}$$

and for the coincidence cross section

$$\frac{d^3\sigma}{d\Omega_1 d\Omega_2 dE_1}=\frac{1}{(2\pi)^6}\frac{1}{3}\int\left[\frac{\tilde{p}_0(\tilde{E}_0+\tilde{E}\,')^2 p_2^2 p_1 E_q}{\tilde{p}_1\tilde{E}\,' p_0\,|\,E_q p_2+p_2E_2-E_2\hat{p}_2\cdot(p_0-p_1)\,|}\right]\left[\frac{d\sigma}{d\tilde{\Omega}}\right]_{pp}\sum_{\substack{m_n,m_{p'}\\ m_6}}|A|^2 d\Omega_{\hat{\kappa}}\,. \tag{19}$$

We thus observe that, as a result of the form of the joint momentum distribution [Eq. (12)],

$$V(\kappa,q)=\frac{1}{3}\sum_{\substack{m_n,m_{p'}\\ m_6}}\int\left|A(m_n,m_{p'},m_6,\mathbf{q},\boldsymbol{\kappa})\right|^2 d\Omega_{\hat{\kappa}}\,, \tag{20}$$

the fourfold cross section factorizes exactly into a product of a kinematic factor (kf), the elastic scattering cross section $[d\sigma/d\tilde{\Omega}]_{pp}$, and the joint momentum distribution $V(\kappa,q)$. In the above equation, the integral over the angle of $\hat{\mathbf{q}}$ is absent since $\hat{\mathbf{q}}$ lies in the direction of $\hat{\mathbf{z}}$. As a result of this factorization, $V(\kappa,q)$ may be extracted from an experiment conducted so as to ensure proton pole dominance.

B. Momentum distribution

The derivation of $V(\kappa,q)$ from a three-body theory is a tedious task, which essentially requires the computation of the overlap integral

$$\langle -\mathbf{q},m_{p'},m_n,\varphi_\kappa^{(-)}(\mathbf{k}_{23})\,|\,\Psi_{m_6}^{[1]}\rangle\,.$$

A detailed description of the calculations is given in Ref. 1. These were done for five different models of the ground state of ^{6}Li, as developed by Lehman, Rai, and Ghovanlou (LRG).[17]

For excitation energies below the value for α-particle breakup (~20 MeV), the ^{6}Li nucleus may be visualized as a system of three particles, npα, where the α is taken as elementary. The basic, so called simple model (SM) employs a $^3S_1$ partial-wave nucleon-nucleon (NN) interaction and the $P_{3/2}$ component of the αN interaction. The 0% and 4% full models (FM) include the dominant αN components at low energies, $S_{1/2}$, $P_{1/2}$, and $P_{3/2}$ and a 0% or 4% $^3D_1$ (tensor) component in the NN interaction, respectively. There are two ways to represent the $S_{1/2}$ αN interaction consistent with the Pauli principle and with low-energy phase shifts. The first is through a purely repulsive potential and the second through an attractive-projected potential with a forbidden bound state removed.[18,19] The same model and corresponding parameters are used for both the ground state of ^{6}Li and the final nα scattering state, to assure full consistency of the calculations. Details as to the form of the wave functions and underlying potentials may be found in Ref. 1.

C. Kinematics

The t matrix $\langle \mathbf{p}_1,\mathbf{p}_2\,|\,t\,|\,\mathbf{p}_0,-\mathbf{q}\rangle$ for quasifree pp scattering, which enters the expression for the (p,2p) cross section, is properly half off-the-energy shell. In the equations for the fourfold and threefold differential cross section, Eqs. (18) and (19), we have replaced the t matrix by a free c.m. pp cross section. An ambiguity arises, however, in the choice of an on-shell energy, because the intermediate proton, p′, is off its mass-energy shell (Fig. 2) in quasifree scattering.

Various on-shell approximations or prescriptions can be used to calculate the c.m. cross section $[d\sigma/d\tilde{\Omega}]_{pp}$. One is the "final-state" prescription, in which the known energies and momenta of the outgoing particles are used to calculate the on-shell kinetic energy $E_{\text{on-shell}}$, of the initial proton. Also needed are the c.m. scattering angle, $\theta_{\text{c.m.}}$, and the c.m. momenta, $\tilde{p}_0$ and $\tilde{p}_1$, which enter into the kinematic factor. The relativistic invariant $S=(P_1+P_2)^2$ is used to transform from the laboratory to the c.m. frame:

$$S=2M^2c^4+2E_1E_2-2\hbar^2c^2p_1p_2\cos(2\theta)\,, \tag{21a}$$

$$\tilde{p}_0=\left\{\frac{[2E_0(E_1+E_0)-2\hbar^2c^2\cos\theta p_0(p_1+p_2)]^2-M^2c^4}{\hbar^2c^2 4S}\right\}^{1/2}, \tag{21b}$$

$$\tilde{p}_1=(\tfrac{1}{2})[S-4M^2c^4]^{1/2}\,, \tag{21c}$$

$$\cos\theta_{\text{c.m.}}=\frac{2p_0p_1\hbar^2c^2\cos\theta-2E_0E_1+2\tilde{E}_0\tilde{E}_1}{2\hbar^2c^2\tilde{p}_0\tilde{p}_1}\,. \tag{21d}$$

The on-shell momentum of the incoming proton is obtained by solving the quadratic equation:

$$p_0^2\hbar^2c^2[(E_1+E_0)^2-\hbar^2c^2\cos^2\theta(p_1+p_0)^2]-S\hbar^2c^2\cos\theta(p_1+p_2)p_0-\frac{S^2}{4}+M^2c^4(E_1+E_0)^2=0\,, \tag{22}$$

which has only one physical solution.

The energies and momenta of the outgoing protons are obtained by solution of the momentum and energy conservation equations for the reaction [cf. Fig. 1(b)]

$p_0+{}^6\mathrm{Li}\rightarrow p_1+p_2+(n\alpha)$:

$$p_0+q\cos\psi=(p_1+p_2)\cos\theta\ , \tag{23a}$$

$$p_1\sin\theta=p_2\sin\theta+q\sin\psi\ , \tag{23b}$$

$$T_0=T_1+T_2-B_6+\frac{q^2}{10M}+\frac{\kappa^2}{2\mu_{n\alpha}} \tag{23c}$$

where T_0, T_1, and T_2 are the kinetic energies of the incoming and outgoing protons. In the relevant experimental geometry, $k_1=k_2$, $\psi=0$, and Eqs. (23) simplify to

$$q=2p_1\cos\theta-p_0\ , \tag{24a}$$

$$T_0=2T_1-B_6+\frac{q^2}{10M}+\frac{\kappa^2}{2\mu_{n\alpha}}\ . \tag{24b}$$

In the "initial state" prescription, we employ knowledge of E_0 and E_q [obtained from solution of Eqs. (24)], to transform to a reference frame in which $q=0$:

$$S=2M^2c^4+2E_{(\text{on-shell})}Mc^2\ , \tag{25a}$$

$$S=2M^2c^4+2E_0E_q-2\hbar^2c^2p_0q\ . \tag{25b}$$

Therefore,

$$E_{(\text{on-shell})}=\frac{E_0E_q-\hbar^2c^2p_0q}{Mc^2}\ , \tag{26a}$$

$$\hbar ck_{(\text{on-shell})}=(E^2_{(\text{on-shell})}-M^2c^4)^{1/2}\ , \tag{26b}$$

$$p_1'=\frac{p_{(\text{on-shell})}}{2\cos\theta}\ , \tag{26c}$$

where p_1' is the momentum of the outgoing protons, used in the transformation to the c.m. frame. The form of the equations for $\tilde{p}_0$, $\tilde{p}_1$, and $\cos\theta_{\text{c.m.}}$ is the same as in the final state prescription.

A third prescription is given by the pseudopotential model introduced by Lim and McCarthy.[20] In this model, $[d\sigma/d\tilde{\Omega}]_{pp}$ becomes equal to the on-shell cross section at the laboratory energy

$$E_{\text{lab}}=(\tfrac{1}{2})(E_{\text{final}}+E_{\text{initial}})\ . \tag{27}$$

Therefore, this method is also referred to as the "average energy" prescription.

The c.m. pp scattering angle is roughly 90° for all three prescriptions. However, the on-shell energy for the initial state prescription is clearly larger (because we assume a stationary target proton) than that for the final state prescription. Now, at $\theta_{\text{c.m.}}=90°$, the pp cross section decreases monotonically with increasing incident energy,[21] certainly up to $\sim$170 MeV. We therefore expect that

$$\sigma_{\text{initial}}\leq\sigma_{\text{average}}\leq\sigma_{\text{final}}\ .$$

Redish *et al.*[22] showed that, in a symmetric angle geometry, the half-off-shell cross section is close to the prediction of the "average energy" on-shell prescription. Also, it was proven by Bhowmik[10] that, for reactions near 100 MeV, the difference between the various prescriptions increases for decreasing angle and increasing relative energy, E_κ. The off-shell ambiguity is further diminished at higher energies because of the flatness of the pp cross sections beyond 150 MeV.[21]

In the present work, the final state prescription was chosen because the outgoing momenta and energies are well known through measurements. However, the choice of the on-shell prescription is more or less arbitrary and not critical for small q values. For purposes of comparison, the initial state prescription was also used in the calculation of one of the binding energy spectra of the Maryland experiment ($E_0=100$ MeV, $\theta=35.4°$). Results will be discussed in the next section.

The on-shell elastic cross section, $[d\sigma/d\tilde{\Omega}]_{pp}$, was computed by a subroutine developed by N. Chant at the University of Maryland. Inserted into the program are the z component of total isospin of the system (1 for pp), the on-shell laboratory kinetic energy in MeV, and the c.m. scattering angle in degrees. Nucleon-nucleon scattering observables are subsequently computed from sets of phase shift data. Up to 500 MeV, the data are derived from Arndt, March 1977. For pp scattering above 500 MeV, they come from Arndt's empirical fit of October, 1977, including the Argonne resonance data.

D. Energy averaging over E_1

The binding energy spectrum is a plot of coincident events versus E_κ for a given pair of symmetric angles θ. Theoretically, the kinematics are chosen such that $E_1=E_2$, represented by a straight line on a two-dimensional plot of E_1 *vs* E_2. In reality, however, this condition can hardly ever be precisely fulfilled. For this reason, Bhowmik and co-workers used the following procedure in order to improve statistics.[10] All events bounded by the region $E_1-E_2=\pm10$ MeV ($|E_1-E_2|\leq10$ MeV) were projected onto the line $E_1=E_2$ and summed as a function of proton separation energy, E_s, to obtain a binding energy spectrum.

In order to find the difference this would make, a similar method was used to theoretically duplicate the experimental averaging technique. The energy averaged cross section is defined as

$$\bar{\sigma}=\int_{E_{\min}}^{E_{\max}}\frac{\sigma(E_1)dE_1}{(E_{\max}-E_{\min})}\ , \tag{28}$$

where $E_{\max}$ and $E_{\min}$ represent the maximum and minimum values of E_1 for which the condition $|E_1-E_2|\leq10$ MeV holds.

The energy averaging procedure did not greatly alter the results of an exact ($E_1=E_2$) calculation of $d^4\sigma$, mainly because the kf depends on the sum (E_1+E_2), which remains constant as the difference (E_1-E_2) varies.

E. Energy resolution

In any experiment the outgoing particle energies cannot be detected with infinite precision. Rather, there is a resolution which limits the measurement and which is characteristic of the detectors. Any theoretical calculation destined for comparison against experiment must take into account the finite energy resolution. In the Maryland experiment of Bhowmik,[10] for instance, the spectrometer resolution was 1 MeV. In order to compare with their data, the following method was used to "fold" the resolution into the theoretical cross section.

Assuming the finite resolution is due to random statistical fluctuations, the folding function may be represented by a Gaussian whose full width at half maximum (FWHM) is 1 MeV:

$$F(E,E_\kappa;\Delta\epsilon)=\frac{2\sqrt{\ln 2}}{\sqrt{\pi}\Delta\epsilon}\exp\left[-\frac{4\ln 2(E-E_0)^2}{(\Delta\epsilon)^2}\right], \tag{29}$$

where $\Delta\epsilon$ is the FWHM and the function $F(E,E_\kappa;\Delta\epsilon)$ is normalized to unity:

$$\int_{-\infty}^{\infty} F(E,E_\kappa;\Delta\epsilon)dE=1 . \tag{30}$$

The Gaussians are centered at each calculated point of the binding energy spectrum, $\sigma(E_\kappa)$, where $0\le E_\kappa\le 25$ MeV. The "folded" value of the cross section thus becomes

$$\sigma(E_\kappa)=\int_{-\infty}^{\infty} F(E',E_\kappa;\Delta\epsilon)\sigma(E')\theta(E')dE' . \tag{31}$$

where $\theta(E')$ is the step function:

$$\theta(E')=\begin{cases}1, & E'\ge 0\\ 0, & E'<0\end{cases} . \tag{32}$$

A four point Lagrangian interpolation method was used to find $\sigma(E')$ in the intervals between the calculated points. Simpson's rule was then applied to obtain the integral in Eq. (31) numerically. The result was a reduction of $d^4\sigma$, especially in the region of the resonance peak.

F. Coincidence cross section

Two types of threefold coincidence spectra are usually measured in a ^{6}Li(p,2p)nα experiment. As stated previously, the energy sharing spectrum is plotted as a function of q, while the angular correlation spectrum is expressed as a function of θ. The kinematics of the two measurements are different. In the case of the energy sharing spectrum, θ is kept constant while q varies independently. The equations of motion are solved for E_1 and E_2 in terms of q, E_κ, and E_0. Subsequently, $d^3\sigma$ is obtained by integration over some region of E_κ (usually the width of the $\frac{3}{2}$-resonance peak) for each q. The curve is symmetrical about the point $q=0$ under the PWIA and the values of q are the same on both sides. The difference lies in the relative magnitudes of E_1 and E_2. To one side of $q=0$, $E_1>E_2$, and to the other, $E_1<E_2$, while the sum (E_1+E_2) remains constant. The vector $\mathbf{q}$ is not parallel to $\mathbf{p}_0$ but forms an angle $\psi\neq 0$ [Fig. 1(b)] with respect to the incident direction.

If the kinematic factor (kf) and $[d\sigma/d\tilde{\Omega}]_{pp}$ are fairly constant over the range of q values of interest ($0\le q\le 1.4$ fm^{-1}), they may be divided out of $d^4\sigma$ in order to get the momentum distribution [Eq. (19)]. However, the region around $q=0$ is only kinematically attainable for one angle, the quasifree scattering angle θ, at a given E_0. At other angles, there appears a gap around the neighborhood of $q=0$ in the energy sharing spectra.

In the case of the angular correlation spectra the kinematical arrangement is such that $\mathbf{q}$ remains parallel to $\mathbf{p}_0$ and, consequently, E_1 must equal E_2. The fourfold cross section is integrated over a specific region of E_κ for each value of θ.

G. Data

In view of the very good energy resolution and the extensive results obtained in the Maryland experiment, it was considered worthwhile to compare these data to the theoretical results. As mentioned previously, however, the incident energy was too low (100 MeV) to rule out distortion effects. These measurements, therefore, will serve only as a basis for *qualitative* comparison. On the other hand, the higher beam energy of the older Tyren experiment[9] facilitates a more quantitative comparison. Because of the uncertainty as to the energy resolution (see Sec. I), however, this quantitative comparison can only be approximate.

III. RESULTS AND DISCUSSION

A. Binding energy spectra

The results of the ^{6}Li(p,2p)nα calculations are presented in Figs. 3–22. The binding energy spectra for the kinematics of Maryland are plotted in Figs. 3–6, which correspond to four different angle pairs (35.4°, 36.5°, 42.8°, and 47.0°). The open circles represent the experimental points, while the various lines represent the results of the theoretical calculations. A common feature of all four graphs is the reduction of the folded spectra with respect to the bare spectra in the region of the peak, and the rapid convergence of the two thereafter. The sharper the resonance peak, the more dramatic the reduction of the spectrum after the energy resolution is folded in. The areas under the $d^4\sigma$ curve, centered at a particular E_κ, must be the same before and after folding in the resolution. Since the points on either side of a peak are weighed with the peak value, the curve is flattened out, resulting in a smaller value of $d^4\sigma(E_0)_{\text{folded}}$. In Fig. 3, the curve which was energy averaged over $|E_1-E_2|\le 10$ MeV differs very little from the bare spectrum. This results from the constancy of the sum (E_1+E_2) as (E_1-E_2) is allowed to vary.

Three of the theoretical spectra (35.4°, 36.5°, and 47.0°) exhibit a sharp resonance peak at $E_\kappa=0.7$ MeV caused by the dominant $P_{3/2}$ αN interaction. For these three angles, the $P_{1/2}$ contribution is most significant at ~ 2.4 MeV and is concealed in the tail of the $P_{3/2}$ peak,

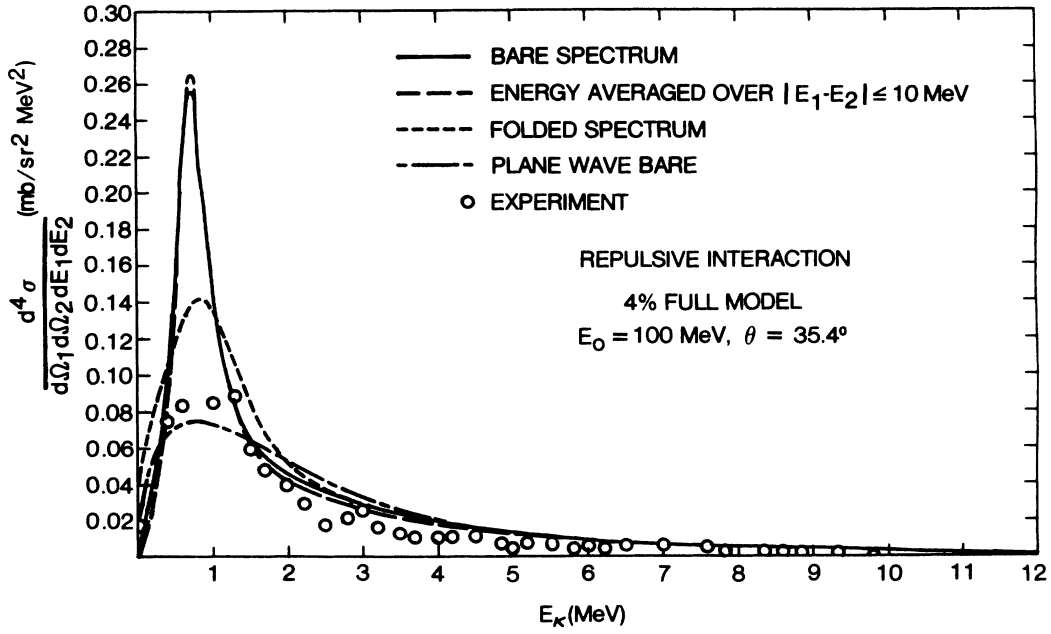

FIG. 3. ^{6}Li(p,2p)nα binding energy spectrum: bare and folded spectra vs experiment ($E_0 = 100$ MeV, $\theta = 35.4°$).

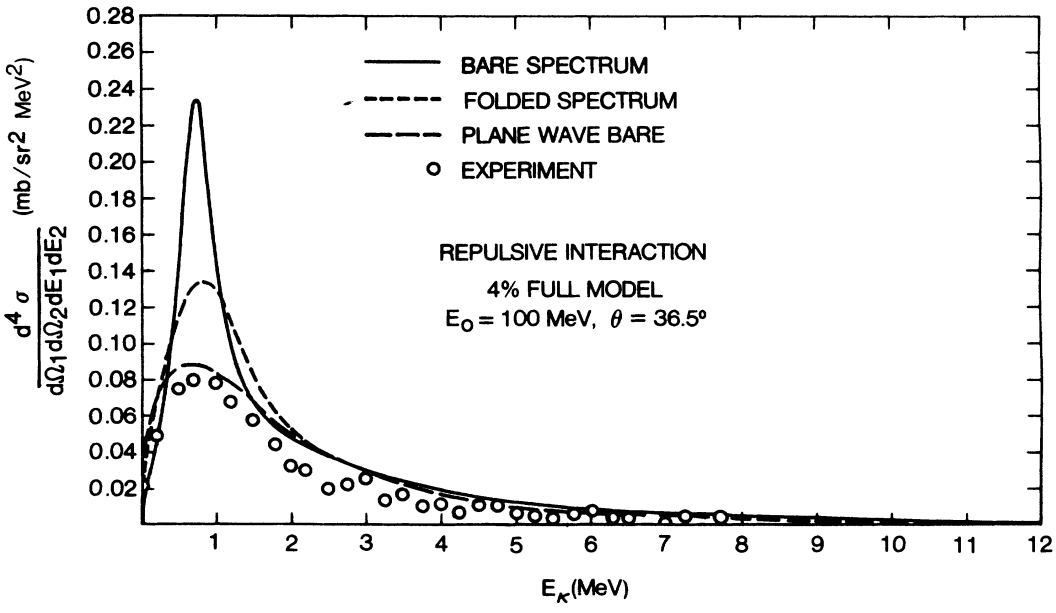

FIG. 4. ^{6}Li(p,2p)nα binding energy spectrum: bare and folded spectra vs experiment ($E_0 = 100$ MeV, $\theta = 36.5°$).

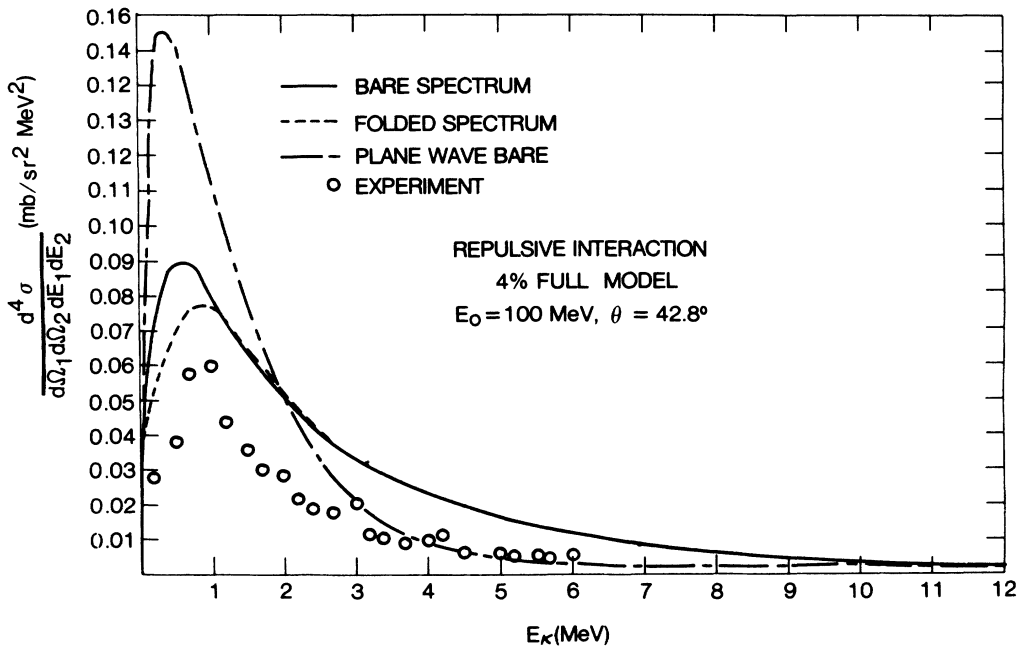

FIG. 5. ^{6}Li(p,2p)nα binding energy spectrum: bare and folded spectra vs experiment ($E_0 = 100$ MeV, $\theta = 42.8°$).

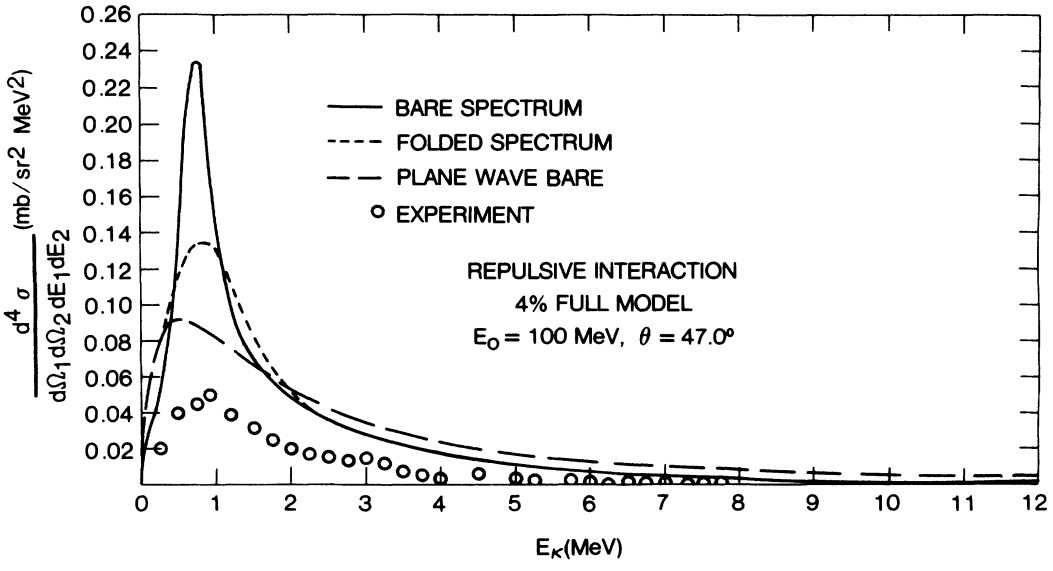

FIG. 6. ^{6}Li(p,2p)nα binding energy spectrum: bare and folded spectra vs experiment ($E_0 = 100$ MeV, $\theta = 47.0°$).

while the nonresonant $S_{1/2}$ interaction increases the cross section at higher E_κ values and lowers it at $E_\kappa \leq 3$ MeV (Fig. 7). We also notice that the binding energy spectrum for the quasifree angle 42.8° exhibits a much broader peak at $E_\kappa = 0.5$ MeV, with a final-state plane-wave contribution that is ~90% higher at the maximum than the full curve. The plane-wave spectra are all smaller than the full curves in the peak region for the other angles. These observations may be attributed to the variation of the momentum distribution with q, which changes as a function of E_κ and θ (See Ref. 1). For the quasifree angle, q is small and "negative" (vector $\mathbf{q}$ parallel to $\mathbf{p}_0$) over the region of the peak ($-0.018 \geq q \geq -0.029$ fm^{-1} for $0 \leq E_\kappa \leq 1$ MeV). At $\theta = 47.0°$, it is still "negative," but larger in magnitude ($-0.177 \geq q \geq -0.188$ fm^{-1}), while for the smaller angles, q is "positive" (vector $\mathbf{q}$ antiparallel to $\mathbf{p}_0$) and steadily decreases over the peak ($0.228 \geq q \geq 0.215$ fm^{-1} at 35.4° while $0.194 \geq q \geq 0.182$ fm^{-1} at 36.5°).

Agreement with experiment seems to be better in the peak region for the quasifree angle 42.8° (PWIA prediction for folded curve is ~25% higher than experiment at peak value whereas for $\theta = 35.4°$ it is ~70% higher). The opposite is true in the tail region. This can be understood by virtue of the fact that, at $E_0 = 100$ MeV, the experiment was optimized to get quasifree kinematics around the resonance. At higher energies, optimization would extend further out into the tail region and better agreement with PWIA results might be expected.

This conjecture is confirmed in Fig. 8, which presents the quasifree binding energy spectrum of Tyren *et al.*[9] At the higher incident energy of 460 MeV, agreement with theoretical predictions is much improved, allowing for the fact that, since the energy resolution was uncertain, one was not theoretically folded into this cross section. On the basis of the above, one may conclude that low energy (p,2p) experiments are not adequate for comparison with PWIA theory, or the best means of extracting the momentum distribution. However, when the incident particle has sufficient energy (≥ 500 MeV) to ensure that the ejected proton leaves the nucleus with a kinetic energy ≥ 100 MeV relative to the $n\alpha$ system, rescattering may be neglected and meaningful comparisons with PWIA calculations may be made.

In Fig. 9, the predictions of the 4% attractive-projected model for $d^4\sigma$ are contrasted with those for the 4% repulsive model. It can be seen in later graphs, as well as in this one, that the attractive $S_{1/2}$ potential gives consistently higher results, especially in the region of the peak, than the repulsive $S_{1/2}$. This can be understood on the basis of the predictions for the binding energy, which for the attractive model is 3.903 MeV vs 4.0624 MeV for the repulsive one. A more tightly bound system makes the knockout of a nucleon by a projectile more difficult, which results in a lower cross section. The difference in the cross sections may also be interpreted as a result of the different properties of the $S_{1/2}$ potentials, which are also included in the final $n\alpha$ state. For $\theta = 42.8°$, the discrepancy between experiment and the attractive-projected value for $d^4\sigma$ is ~40% as opposed to 25% for the repulsive value at the maximum.

Figure 10 compares the predictions of the final state versus the initial state prescriptions for the on-shell proton-proton cross section. The final state result at peak value is ~20% higher than that for the initial state. As discussed in Sec. II C this is a consequence of the fact that $[d\sigma/d\tilde{\Omega}]_{pp}$ decreases monotonically with increasing energy. The on-shell energy E_0 obtained from the final state prescription is smaller than that from the initial state prescription, because in the latter we transform to a frame in which the struck proton is initially stationary. Additionally, the kinematic factor includes the ratio $\tilde{p}_0/\tilde{p}_1$, which is smaller for the initial

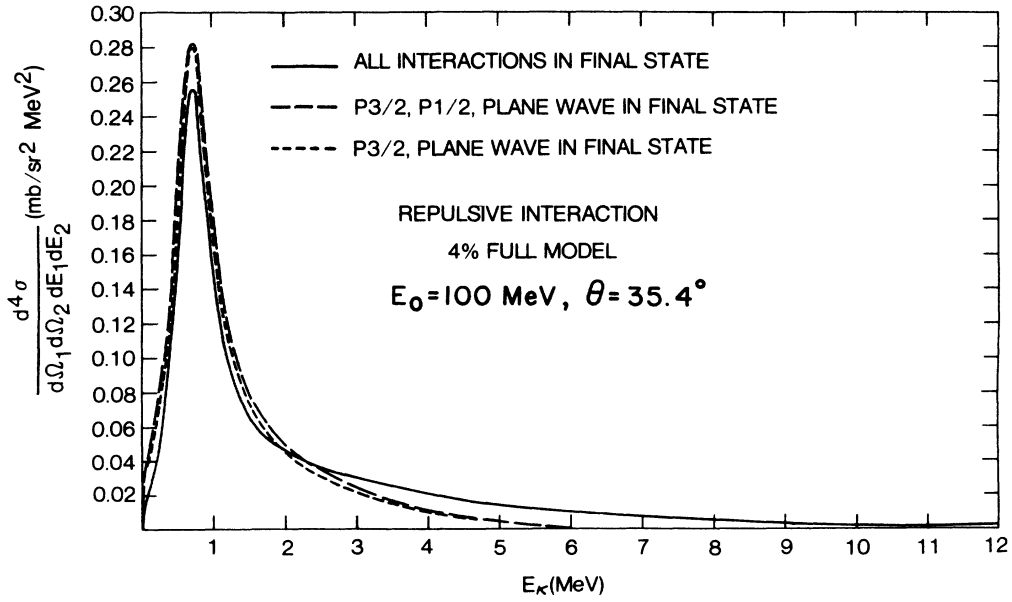

FIG. 7. ^{6}Li(p,2p)nα binding energy spectrum: contributions of nα final state partial wave interactions.

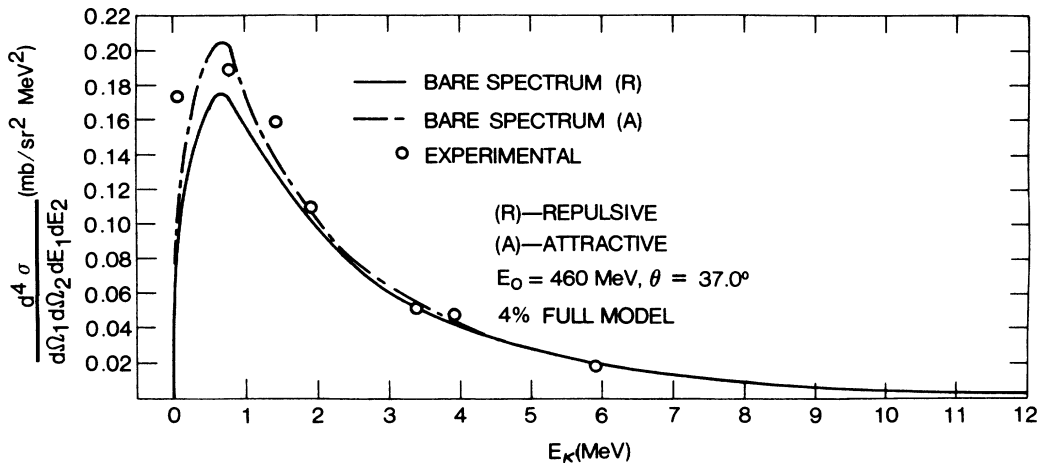

FIG. 8. ^{6}Li(p,2p)nα binding energy spectrum: repulsive and attractive-projected $S_{1/2}$ αN models vs experiment ($E_0=460$ MeV, $\theta=37.0°$).

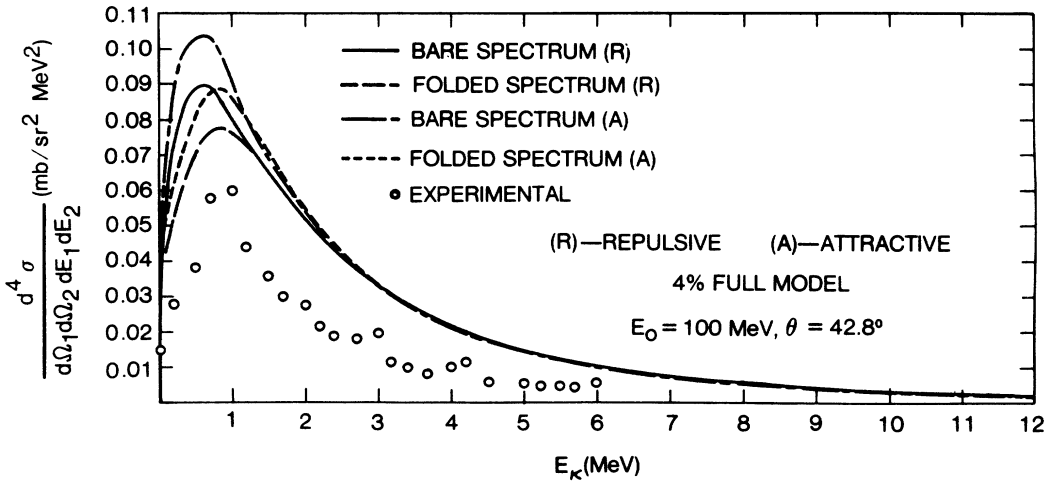

FIG. 9. ^{6}Li(p,2p)nα binding energy spectrum: repulsive vs attractive-projected $S_{1/2}$ models ($E_0=100$ MeV, $\theta=42.8°$).

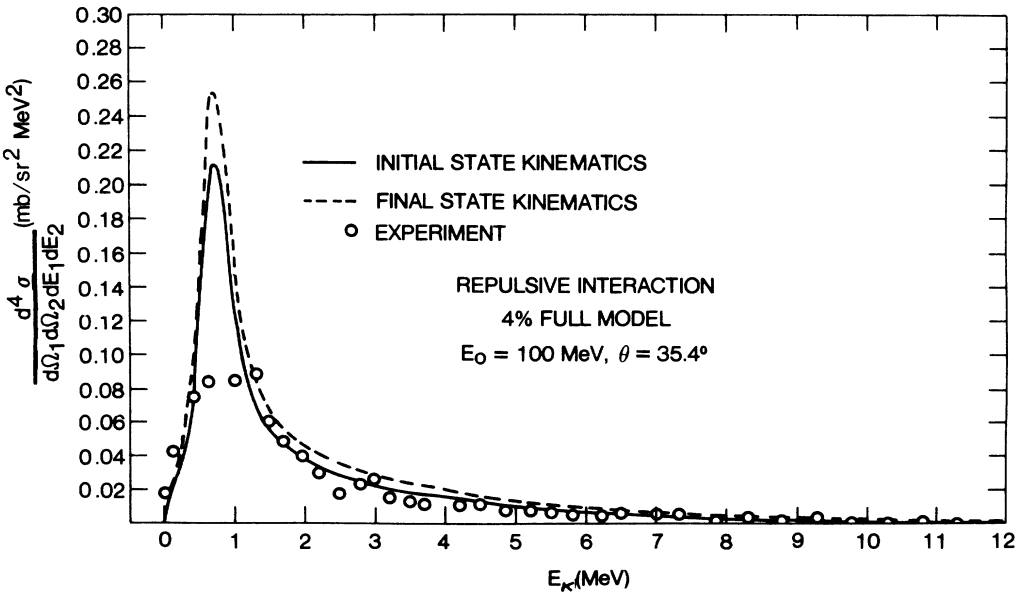

FIG. 10. ^{6}Li(p,2p)nα binding energy spectrum: comparison of prescriptions for $[d\sigma/d\Omega]_{pp}$ (on-shell) initial vs final state kinematics ($E_0=100$ MeV, $\theta=35.4°$).

than the final state prescription. The binding energy curve for the true half-shell t matrix lies somewhere in between the two curves of Fig. 10.[10,22]

Figures 11–14 display the effect of the presence of the $S_{1/2}$ αN interaction on the binding energy spectrum. In Fig. 11, $d^4\sigma$ is presented for the repulsive model (4% FM) and the quasifree angle 42.8°, with and without the $S_{1/2}$ interaction in the final state. Removing the repulsive $S_{1/2}$ potential leads to a much larger cross section in the region of the peak ($\sim$80% higher at peak value) and a much smaller cross section in the region of the tail. The curve without the $S_{1/2}$ interaction seems to die out much faster than the full curve, implying a major $S_{1/2}$ contribution for $E_\kappa \geq 2$ MeV. In the region of the peak, where the relative nα energy is low, removal of the repulsive interaction maximizes the plane-wave contribution, since the $P_{3/2}$ partial-wave adds very little to the quasifree spectrum. In a system with no interactions, it is of course easier to knock out one of the particles. Hence the larger cross section for $E_\kappa \leq 2$ MeV. The same phenomenon is observed for the attractive-projected model, except that the magnitudes of $d^4\sigma$ are larger than for the repulsive model.

If we remove the components in the ground-state wave function that are directly attributable to the $S_{1/2}$ interaction, the cross section becomes even larger (Figs. 13 and 14). The cross section now exhibits an even greater enhancement than it did when the $S_{1/2}$ was removed only in the final state. Again, we see that the main (positive) contribution of the $S_{1/2}$ interaction is in the region beyond $E_\kappa = 2$ MeV.

In Figs. 15 and 16, a comparison is made among the predictions for the cross section based on the various models of ^{6}Li. Figure 15 includes the spectra for the simple model, the repulsive 0% and the repulsive 4% full models. We notice that the 0% FM curve falls below the 4% FM curve everywhere in the E_κ domain of interest. This may be attributed to the binding energy, which is lower for the 4% than the 0% model (4.0624 vs 4.4463 MeV). It has been determined that the root-mean-square np distance is smaller in the ^{6}Li nucleus than it is in the deuteron ($\approx$3.0 vs 3.8 fm).[23] In the deuteron, the tensor force plays a major role in the binding. When it is present, the strength of the central force is reduced compared to the value needed in the absence of the tensor force to yield the correct deuteron binding. Now, in ^{6}Li where the np system (on the average) is closer together than in a deuteron, the role of the tensor force is *diminished*. Therefore, since the strength of the central component is reduced in the presence of the tensor component, we anticipate the *decrease* in the ^{6}Li binding when the np tensor force is present. A lower binding energy implies a more diffuse structure, in which the knockout of a nucleon is facilitated relative to a more tightly bound system. Hence the larger cross section for the 4% FM than the 0% FM (also true for the attractive-projected potential, Fig. 16). At peak value, the SM is smaller than both versions of the FM, due to the absence not only of an np tensor force, but also of the $S_{1/2}$ αN interaction. The spread in the SM peak is a consequence of the increased binding energy (4.67 MeV) relative to the FM, and to more subtle effects, such as the interference between the $P_{1/2}$ and $S_{1/2}$ waves, which are absent in the SM.

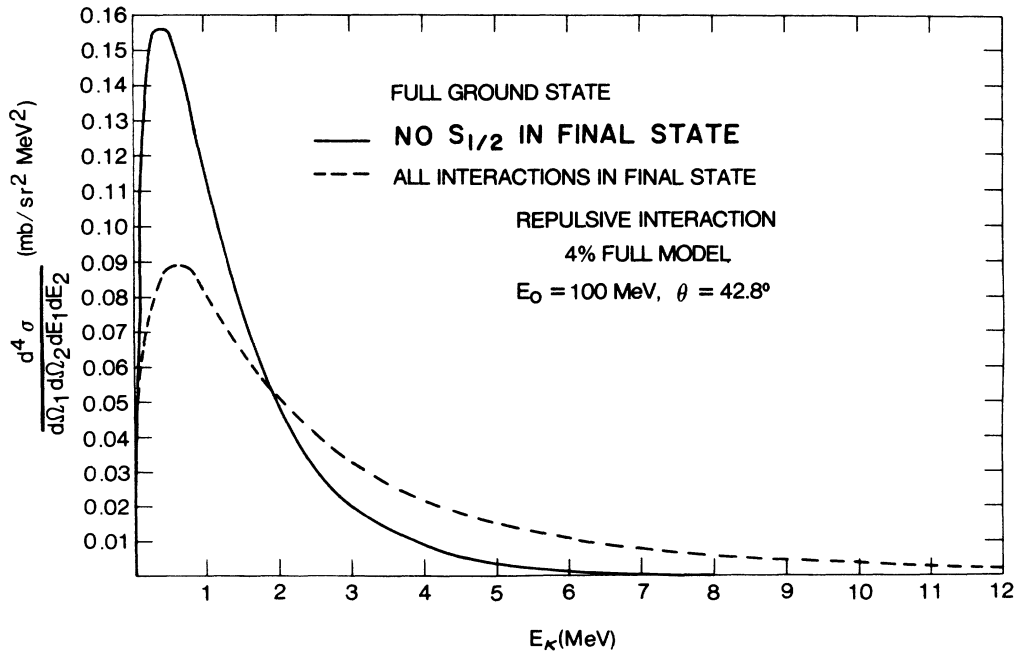

FIG. 11. ^{6}Li(p,2p)nα binding energy spectrum: contribution of $S_{1/2}$ interaction in final state, repulsive model.

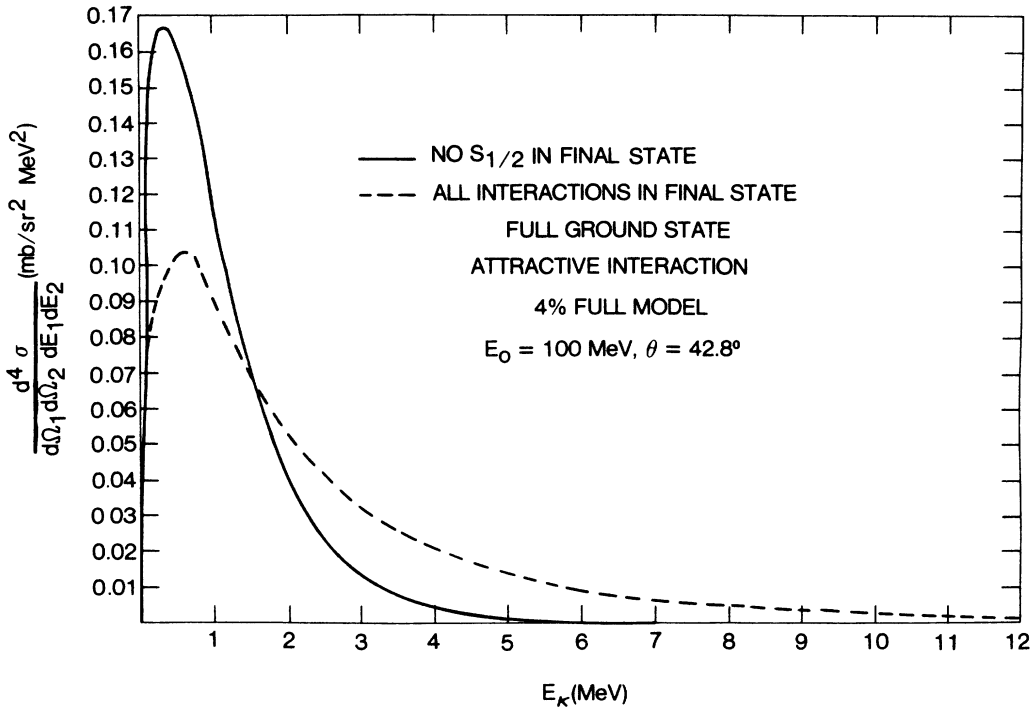

FIG. 12. ^{6}Li(p,2p)nα binding energy spectrum: contribution of $S_{1/2}$ interaction in final state, attractive-projected model.

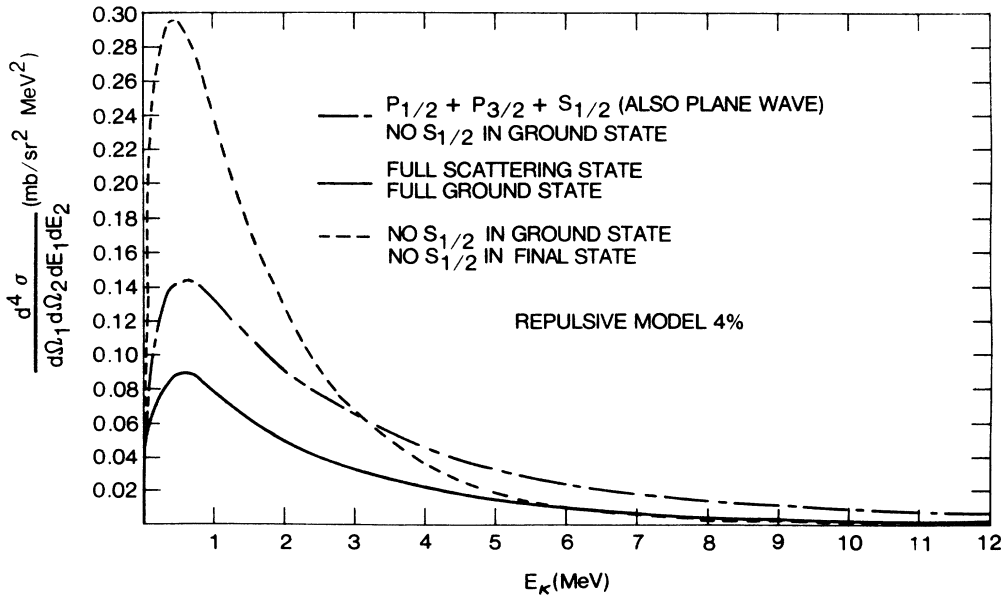

FIG. 13. ^{6}Li(p,2p)nα binding energy spectrum: contribution of $S_{1/2}$ αN interaction in final and ground states, repulsive model (θ=42.8°).

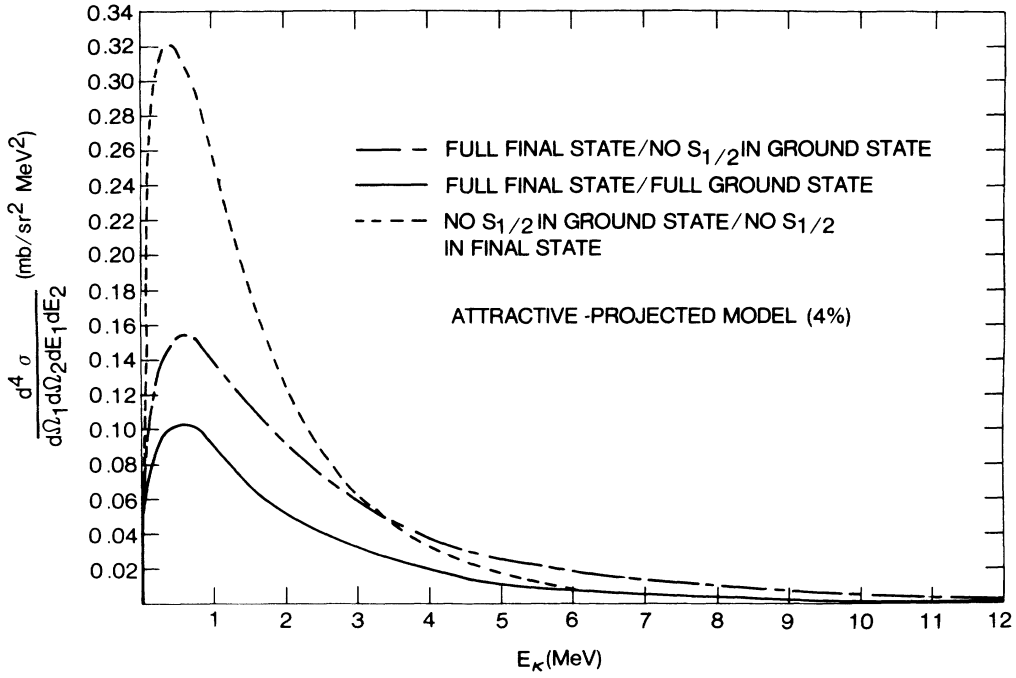

FIG. 14. ^{6}Li(p,2p)nα binding energy spectrum: contribution of $S_{1/2}$ αN interaction in final and ground states, attractive-projected model (θ=42.8°).

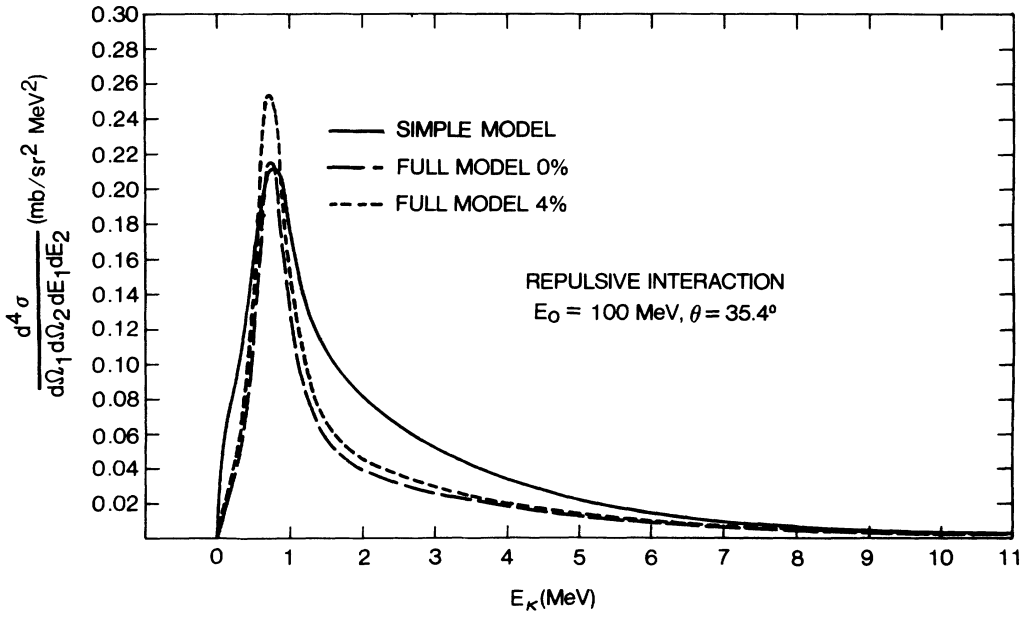

FIG. 15. ^{6}Li(p,2p)nα binding energy spectrum: simple, full (0%) and full (4%) models, repulsive $S_{1/2}$ αN interaction.

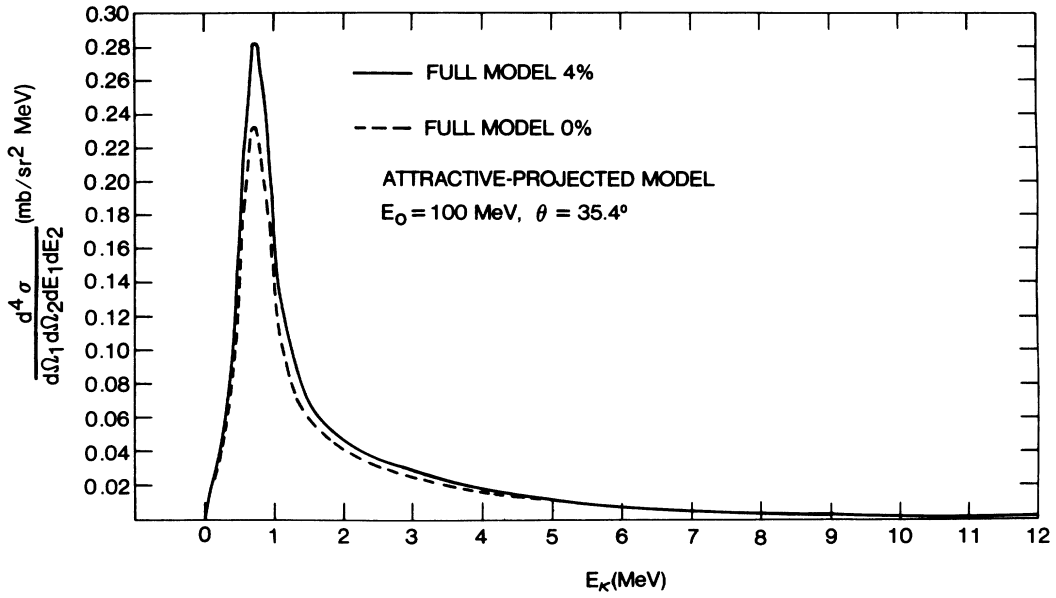

FIG. 16. ^{6}Li(p,2p)nα binding energy spectrum: full (0%) and full (4%) models, attractive-projected $S_{1/2}$ αN interaction.

B. Energy sharing spectra

The threefold cross sections for the kinematics of the Bhowmik experiment are presented in Figs. 17–20. A zero recoil momentum was attainable only for $\theta = 42.8°$, therefore theoretical calculations were carried out for this angle. An energy resolution of 1 MeV was folded into the curves of Figs. 17–22. The range of E_κ integration was 0–2 MeV. The predictions of the repulsive 4% FM are shown and compared with experiment in Fig. 17. Agreement between the full curve (solid line) and the data points (open circles) is better for low q values. At higher q, the experimental distribution becomes narrower than the theoretical one because of rescattering effects both in the initial and the final state.

The relative contributions of the final state interactions are displayed in the same graph. Removal of the $S_{1/2}$ potential (long-dashed line) leads to a higher cross section, especially at low q values. This is in agreement with the analysis of the quasifree binding energy spectrum, which also increases upon elimination of the final state $S_{1/2}$ interaction (Figs. 11 and 12). At higher q values it is the $P_{3/2}$ partial-wave which dominates, therefore the enhancement of $d^3\sigma$ upon removal of the $S_{1/2}$ potential is less drastic for $q \geq 50$ MeV/c. Subtraction of the weaker $P_{1/2}$ wave does not have much of an effect anywhere (dot-dashed curve). Upon removing the $P_{3/2}$ interaction, however, we obtain the plane-wave contribution (short-dashed line), which leads to a maximum at $q = 0$ and decreases monotonically thereafter. The pre-

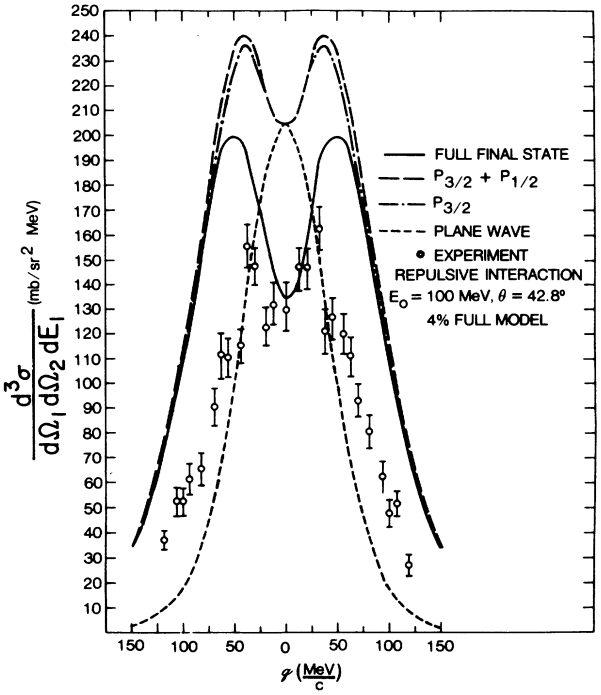

FIG. 17. ^{6}Li(p,2p)nα threefold cross section: contributions of final state αN interactions, theory vs experiment, repulsive $S_{1/2}$ model.

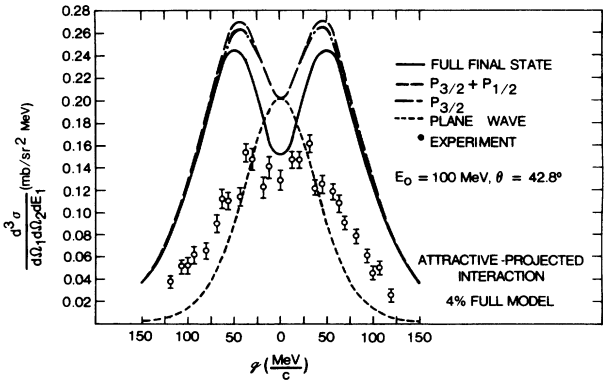

FIG. 18. ^{6}Li(p,2p)nα threefold cross section: contributions of final state αN interactions, theory vs experiment, attractive-projected $S_{1/2}$ model.

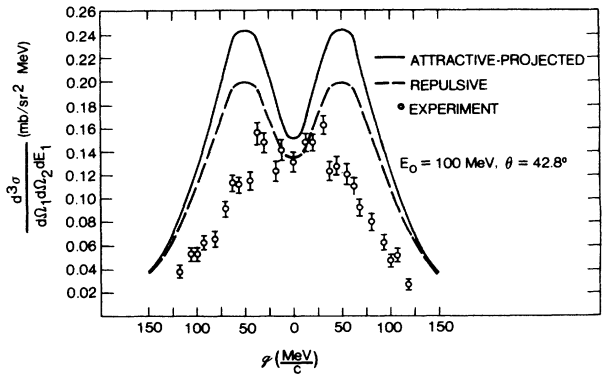

FIG. 19. ^{6}Li(p,2p)nα threefold cross section: comparison of repulsive and attractive-projected $S_{1/2}$ αN models to experiment.

liminary conclusion of this series of computations, then, is that the interference of the plane-wave and $S_{1/2}$ interaction terms is responsible for the "filling" of the dip in the momentum distribution, not the $S_{1/2}$ interaction alone, as previously suggested.[4,10,14] The $S_{1/2}$ interaction, on the contrary, creates more of a minimum relative to the plane-wave case, in the sense that the interference is destructive. The same qualitative results are obtained for the attractive-projected model in Fig. 18.

In Fig. 19, a comparison is made between experiment and the predictions of the two forms of the $S_{1/2}$ potential, which we see are quite distinct. As in the case of the binding energy spectrum, the attractive model leads to a higher value of $d^3\sigma$ than the repulsive model—22% higher at the peak and 12.7% higher at the central minimum. The predicted peak to valley ratios are 1.49, 1.62, 1.24 for the repulsive $S_{1/2}$ model, the attractive-projected $S_{1/2}$ model and the experimental curve, respectively.

The SM was used to obtain the theoretical curves of Fig. 20. Without the $S_{1/2}$ interaction present either in the ground or the final state, there is a conspicuous absence of a minimum. Rather, a maximum in $d^3\sigma$ is observed at $q=0$, which, as seen by removing the final $P_{3/2}$ interaction (dotted curve), is totally attributable to the plane wave.

This point is dramatically emphasized upon subtraction of the plane wave from the full wave curve (dashed line). Here, the absolute minimum predicted by the p-shell shell model of ^{6}Li is clearly noticeable, with the maxima of the $P_{3/2}$ interaction placed symmetrically on either side of $q=0$. The conclusion that the $S_{1/2}$ partial-wave, which is totally absent in the SM, is only partially responsible for the filled minimum in the momentum distribution curve becomes inescapable. To further confirm this, the cross section for the 4% FM was again plotted in Fig. 21 (full line). After this, the components in the wave function directly associated with the $S_{1/2}$ interaction were first removed in the ground state (dashed curve) and then also in the final state (long-short dashed curve). The resulting distribution is identical in shape to the one for the SM.

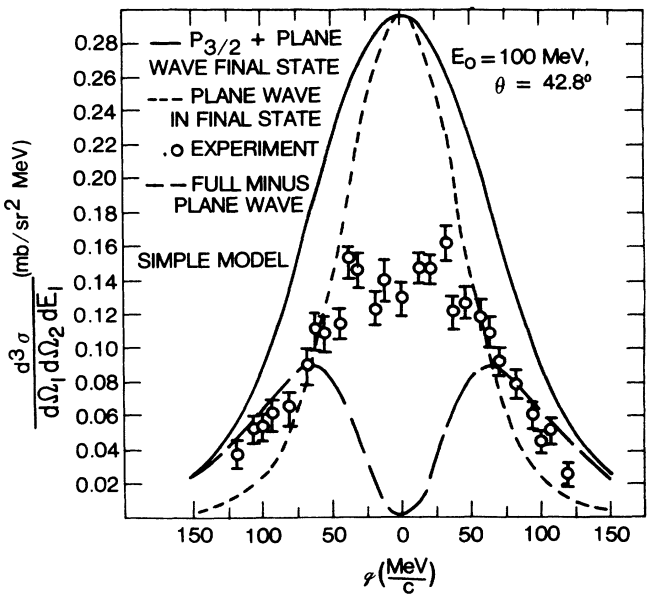

FIG. 20. ^{6}Li(p,2p)nα threefold cross section: contributions of final state αN interactions, simple model, comparison to experiment.

The angular correlation spectrum was calculated for the domain of θ values used by Bhowmik and Chang for an incident energy of 100 MeV (Fig. 22). The cross section $d^3\sigma$ was integrated over $0 \leq E_\kappa \leq 1.5$ MeV for each q value. We notice, first of all, a slight dip in the spec-

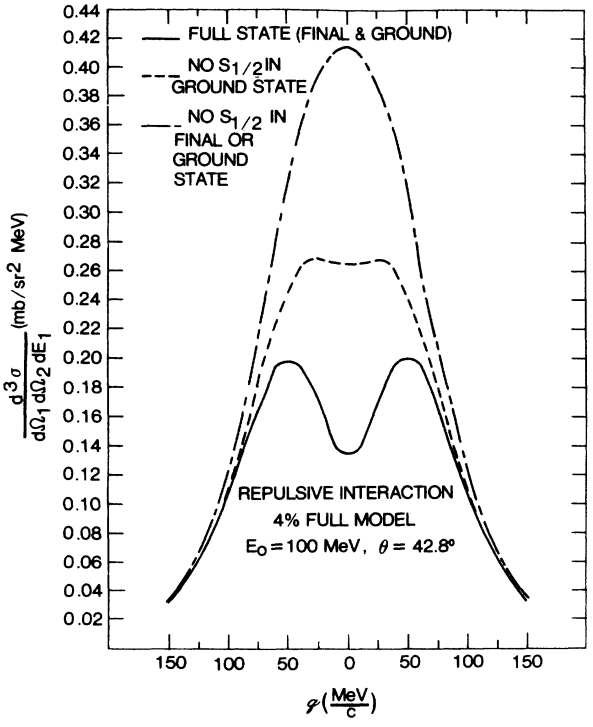

FIG. 21. ^{6}Li(p,2p)nα threefold cross section: contributions of $S_{1/2}$ αN interaction in final and ground state, repulsive model.

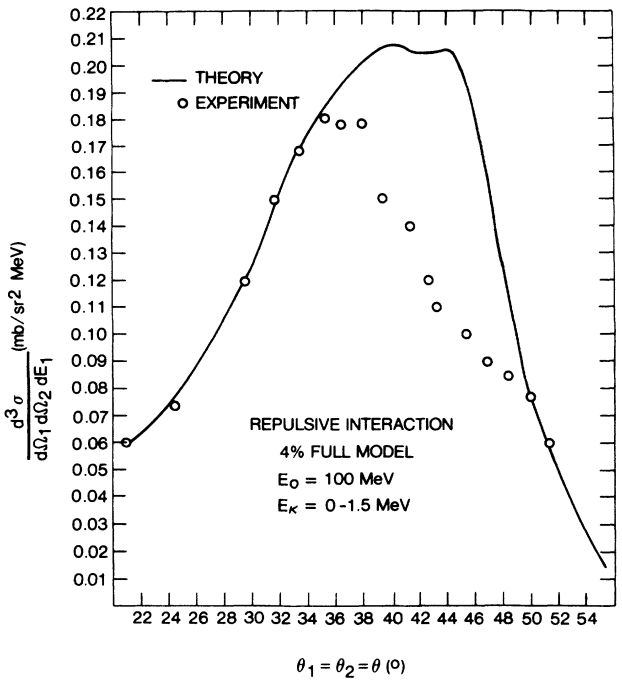

FIG. 22. ^{6}Li(p,2p)nα angular correlation spectrum ($E_0=100$ MeV, $E_\kappa=0$–1.5 MeV).

trum at $\theta\approx 42°$, which corresponds to the quasifree scattering angle. Also, agreement with experiment appears to be quite good for values of $\theta\leq 36°$ and $\theta\geq 50°$. In between, the theoretical analysis predicts a higher cross section than that actually measured, with a shift of the minimum to a lower θ value.

IV. CONCLUSIONS

The significance of this work lies in the use of a complete three-body model of ^{6}Li to calculate the ^{6}Li→p+(nα) vertex amplitude and, in turn, the ^{6}Li(p,2p)nα cross section. Previous theoretical efforts treated the ^{6}Li nucleus mostly as an effective two-body system, excluding the important three-body component. In some cases the final nα state was correctly considered as an unbound system and the predominant low-energy partial-wave interactions were included in the dynamics. The effect of the nα plane-wave final-state component was either not studied separately or was omitted altogether. As the present work has shown, in certain kinematic regions the plane-wave component plays an important role in the p+(nα) momentum distribution.

The three-body approach goes beyond effective two-body methods in producing a complete wave function from optimal representations of the two-body interactions. The LRG model used in the present calculations is based on two-body αN and NN interactions in the ^{6}Li subsystems. These interactions are represented by separable, nonlocal potentials containing parameters which are set by fits to low-energy data for the deuteron and low-energy αN phase shifts. Thereafter, these parameters remain fixed so that the predictions of the model are definite and uniquely determined by the underlying dynamics. Unlike some phenomenological schemes, which were previously used to fit the ^{6}Li→p+(nα) vertex functions to experiment, there remain no free parameters which have to be adjusted in the end. In addition, the Schrödinger equation for the ^{6}Li wave function is translationally invariant so that corrections due to the motion of the c.m. as in oscillator models, are not required.

The predictions of the LRG three-body model concerning the ^{6}Li(p,2p)nα reaction may be summarized as follows:

(1) For angles away from the quasifree scattering angle, the binding energy spectrum is dominated by the $P_{3/2}$ αN resonance peak at $E_\kappa=0.7$ MeV. The final state, $P_{1/2}$ αN interaction is relatively weak and is concealed in the tail of the $P_{3/2}$ spectrum with the main contribution around 2.4 MeV. The $S_{1/2}$ αN interaction is significant mainly at $E_\kappa>2$ MeV, while the plane-wave contribution is smaller than the full wave in the region of the $P_{3/2}$ peak.

(2) The quasifree spectrum is dominated by the $S_{1/2}$ αN interaction and the plane-wave component, which gives larger results than the full wave component in the peak region below $E_\kappa=3$ MeV. At higher E_κ values, the plane-wave curve dwindles rapidly compared to the full-wave curve.

(3) The predictions of the attractive-projected $S_{1/2}$ αN model are consistently higher than those of the repulsive model, for both binding energy and energy sharing spectra. Coincidence experiments with good resolution could distinguish between the two forms of the $S_{1/2}$ potential. This would help in determining which form best represents the dynamics of the ^{6}Li nucleus.

(4) It is the plane-wave term of the final state nα wave function which is mainly responsible for the filling of the $P_{3/2}$ minimum in the p+(nα) momentum distribution at $q=0$. This contradicts Watson's model,[12] according to which the plane wave is negligible compared to the scattered wave in the neighborhood of a resonance. As explicitly demonstrated in Ref. 1, in this case Watson's model does not hold. The $S_{1/2}$ partial-wave αN term destructively interferes with the plane-wave term to reduce the minimum further.

(5) Because of large rescattering effects, the (p, 2p) reaction below 300 MeV does not provide a suitable basis of comparison with PWIA calculations. At 100 MeV incident energy, the outgoing proton energies are roughly 45 MeV each, not large enough to avoid strong interactions between the two protons and also between a proton and the residual nucleus. At higher proton energies (>500 MeV) significant distortion effects may be eliminated.

In view of the fact that (p, 2p) cross sections are four orders of magnitude larger than (e,e'p) cross sections, it is easier to obtain good statistical accuracy by using a proton beam rather than an electron beam. Therefore, facilities such as TRIUMF (Vancouver, B.C.) or LAMPF (Los Alamos, N.M.), which feature high energy proton beams (500 and 800 MeV, respectively) may be ideal for the future realization of ^{6}Li(p,2p)nα experi-

ments from which meaningful results may be derived. The prospect of testing the three-body PWIA predictions against such good sets of data is truly exciting.

The work of the authors was supported in part by the U.S. Department of Energy under Grant No. DE-FG05-86-ER40270.

*Present address: Naval Research Laboratory, Code 4651, Washington, D.C. 20375.

[1]C. T. Christou, D. R. Lehman, and W. C. Parke, Phys. Rev. C **37**, 445 (1988).

[2]C. T. Christou, D. R. Lehman, and W. C. Parke, Phys. Rev. C **37**, 477 (1988).

[3]G. Jacob and Th. A. J. Maris, Nucl. Phys. **31**, 139 (1962); Rev. Mod. Phys. **38**, 121 (1966).

[4]S. Saito, J. Huira, and H. Tanaka, Prog. Theor. Phys. **39**, 635 (1968).

[5]J. P. Garron, J. C. Jacmart, M. Riou, C. Rubla, J. Teillac, and K. Strauch, Nucl. Phys. **37**, 126 (1962).

[6]G. Tibell, O. Sundberg, and P. O. Renberg, Ark. Fys. **25**, 433 (1963).

[7]J. C. Roynette, M. Arditi, J. C. Jacmart, F. Mazloum, M. Riou, and C. Ruhla, Nucl. Phys. **A95**, 545 (1967).

[8]I. A. MacKenzie, S. K. Mark, and Tseh Y. Li, Nucl. Phys. **A195**, 609 (1972).

[9]H. Tyren, S. Kullander, O. Sundberg, R. Ramachandran, P. Isacsson, and T. Berggren, Nucl. Phys. **79**, 321 (1966).

[10]R. K. Bhowmik, C. C. Chang, P. G. Roos, and H. D. Holmgren, Nucl. Phys. **A226**, 365 (1974).

[11]D. R. Lehman and Mamta Rajan, Phys. Rev. C **25**, 2743 (1982).

[12]K. M. Watson, Phys. Rev. **88**, 1163 (1952); A. B. Migdal, Zh. Eksp. Teor. Fiz. **28**, 3 (1955); see also E. W. Schmid and H. Ziegelmann, *The Quantum Mechanical Three-Body Problem* (Pergamon, Oxford, 1974), p. 112.

[13]C. C. Chang, R. Bhowmik, N. S. Chant, and P. G. Roos, University of Maryland, Technical Report No. 76-039 (Physics paper No. 76-008) 1976 (unpublished).

[14]F. Prats, Nucl. Phys. **A227**, 469 (1974).

[15]R. P. Feynman, *Quantum Electrodynamics* (Benjamin/Cummings, 1962) pp. 78–81.

[16]I. S. Shapiro, Institute of Theoretical and Experimental Physics Report, Moscow, U.S.S.R.; I. S. Shapiro, Usp. Fiz. Nauk **92**, 549 (1968) [Sov. Phys. Usp. **10**, 515 (1968)].

[17]Mamta Rai, D. R. Lehman, and A. Ghovanlou, Phys. Lett. **B59**, 327 (1975); D. R. Lehman, Mamta Rai, and A. Ghovanlou, Phys. Rev. C **17**, 744 (1978); A. Ghovanlou and D. R. Lehman, *ibid.* **9**, 1730 (1974).

[18]V. M. Krasnopol'skii and V. I. Kukulin, Yad. Fiz. **20**, 883 (1974) [Sov. J. Nucl. Phys. **20**, 470 (1975)].

[19]D. R. Lehman, Phys. Rev. C **25**, 3146 (1982); I. H. Sloan, Phys. Lett. **B34**, 243 (1971).

[20]K. C. Lim and I. E. McCarthy, Phys. Rev. Lett. **10**, 529 (1963).

[21]E. Segrè, *Nuclei and Particles* (Benjamin, New York, 1977) p. 402.

[22]E. F. Redish, G. J. Stephenson, and G. M. Lerner, Phys. Rev. C **2**, 1665 (1970).

[23]L. Vegh and J. Ero, Phys. Rev. C **23**, 2371 (1981).